Biogeosciences

Research article

Calcification response of reef corals to seasonal upwelling in the northern Arabian Sea (Masirah Island, Oman)

Philipp M. Spreter[1], **Markus Reuter**[2], **Regina Mertz-Kraus**[3], **Oliver Taylor**[4], **and Thomas C. Brachert**[1]

[1]Institut für Geophysik und Geologie, Universität Leipzig, Talstraße 35, 04103 Leipzig, Germany
[2]Institut für Geographie und Geologie, Universität Greifswald, Friedrich-Ludwig-Jahn-Str. 17a, 17489 Greifswald, Germany
[3]Institut für Geowissenschaften, Johannes Gutenberg-Universität Mainz, Johann-Joachim-Becher-Weg 21,
55128 Mainz, Germany
[4]Five Oceans Environmental Services, Villa 1756, Way 3021, Shatti Al Qurm, Muscat, Sultanate of Oman

Correspondence: Philipp M. Spreter (philipp.spreter@uni-leipzig.de)

Abstract. Tropical shallow-water reefs are the most diverse ecosystems in the ocean. Their persistence rests upon adequate calcification rates of the reef building biota, such as reef corals. Coral calcification is favoured in oligotrophic environments with high seawater saturation states of aragonite (Ω_{sw}), which leads to an increased vulnerability to anthropogenic ocean acidification and eutrophication. Here we present *Porites* calcification records from the northern Arabian Sea upwelling zone and investigate the coral calcification response to low Ω_{sw} and high nutrient concentrations due to seasonal upwelling. The calcification rate was determined from the product of skeletal extension rate and bulk density. Skeletal Ba/Ca and Li/Mg proxy data were used to identify skeletal portions that calcified during upwelling and non-upwelling seasons, respectively, and to reconstruct growth temperatures. With regard to sub-annual calcification patterns, our results demonstrate compromised calcification rates during the upwelling season. This is due to declining extension rates, which we attribute to light dimming caused by high primary production. Interestingly, seasonal variations in skeletal density show no relationship with temporally low Ω_{sw} during upwelling. This suggests relatively constant, year-round saturation states of aragonite at the site of calcification (Ω_{cf}) independent of external variability in Ω_{sw}. Although upwelling does not affect seasonal density variability, exceptionally low mean annual density implies permanent Ω_{cf} adjustment to the lowest sub-annual Ω_{sw} (e.g. upwelling). In the Arabian Sea upwelling zone, the mean annual calcification rate is similar to *Porites* from non-upwelling regions because low skeletal density is compensated by high extension growth. Variable responses of reef coral extension to nutrients, which either exacerbate or compensate negative effects of diminished skeletal density associated with ocean acidification, may therefore be critical to the maintenance of adequate carbonate accumulation rates in coral reefs under global change.

1 Introduction

Tropical coral reefs are the most diverse aquatic ecosystems on the planet (Hughes et al., 2017). Their basic building blocks are the calcareous (aragonite) skeletons of symbiotic scleractinian corals (reef corals), and sustained precipitation of skeletal carbonate (calcification) is fundamental for maintaining their structure and function (Perry et al., 2012). Optimum calcification of reef corals is found in oligotrophic water masses of temperatures between 21 to 29.5 °C and a saturation state of seawater with respect to aragonite > 3.3 (Ω_{sw}) (Kleypas et al., 1999). Anthropogenic greenhouse gas emissions threaten reef coral calcification by increasing sea surface temperature (SST) and by causing ocean acidification. In addition, land use, discharge of wastewater and fish farming turn the near-shore shallow-marine environments towards more eutrophic conditions. The responses of reef coral calcification to the rapidly changing environment are highly variable and remain a matter of intense research (Cornwall et al., 2021; Guan et al., 2020; Hall et al., 2018).

The coral calcification rate ($g\,cm^{-2}\,yr^{-1}$) is the product of the linear extension rate ($cm\,yr^{-1}$) measured along the axis of maximum growth and bulk density ($g\,cm^{-3}$) (Dodge and Brass, 1984). The linear extension rate in reef corals is linked to the efficiency of photosynthesis in symbiotic micro-algae, providing energy to the host for upward growth of the skeleton (Muscatine et al., 1981; Sun et al., 2008). Availability of light and water temperature are the main drivers controlling photosynthetic efficiency and thus are positively related to the extension rate (Al-Rousan, 2012; Logan and Tomascik, 1991; Lough and Barnes, 2000). At certain taxon-specific threshold temperatures, however, extension rate declines rapidly due to thermal stress for the micro-algae symbionts (Cantin et al., 2010). Due to sub-annual variations in extension rate, skeletal portions of high and low density are formed, with high-density bands (HDBs) coinciding with low extension rate (and vice versa for low-density bands – LDBs) (DeCarlo and Cohen, 2017; Highsmith, 1979; Klein and Loya, 1991; Knutson et al., 1972). In addition, arago-nite saturation of the calcifying fluid (Ω_{cf}) determines bulk skeletal density (Mollica et al., 2018). Ω_{cf} is approximately 5 times higher than the aragonite saturation of the external seawater (Ω_{sw}), and long-term changes in Ω_{sw} due to ocean acidification lead to declining Ω_{cf} (McCulloch et al., 2017; D'Olivo et al., 2019). Intra-annually, corals are, however, able to maintain relatively stable levels of Ω_{cf} largely independent of short-term variations in Ω_{sw} by upregulating their internal pH_{cf} and DIC_{cf} pool (McCulloch et al., 2017; De-Carlo et al., 2018; D'Olivo and McCulloch, 2017; Ross et al., 2019a).

Near-shore coral reefs are increasingly exposed to anthropogenic eutrophication induced by land use, fish farming and sewage disposal (Lapointe and Clark, 1992; Chen et al., 2019; Chen and Yu, 2011). Eutrophication can have both beneficial and detrimental effects on coral growth, depending on the type of nutrients and their concentration (Tomascik and Sander, 1985; Tomascik, 1990). In general, reef corals are highly adapted to oligotrophic waters with micro-algae symbionts to allow an efficient use of essential nutrients (Muscatine and Porter, 1977). This enables outcompeting other fast-growing biota on a reef whose growth is inhibited by the undersupply of nutrients (Vermeij et al., 2010; Barott and Rohwer, 2012). Strong eutrophication disturbs this adaptive advantage, leading to harmful algal blooms followed by reef coral mass mortality and reef destruction due to the increasing abundance of bioeroders (Al Shehhi et al., 2014; Hallock, 1988). However, moderate increases in certain nutrients such as ortho-phosphate (PO_4^{3-}) have been shown to promote the linear extension rate (Bucher and Harrison, 2001; Dunn et al., 2012; Koop et al., 2001). The opposite effect is reported for nitrate (NO_3^-) even though the calcification response is less pronounced compared to PO_4^{3-} (Koop et al., 2001). In general, increasing eutrophy is considered to cause reef corals to sacrifice skeletal density for increased extension rate ("stretching modulation of skeletal growth"), which can either lead to enhanced, constant or reduced rates of calcification (Carricart-Ganivet and Merino, 2001; Carricart-Ganivet, 2004; D'Olivo et al., 2013; Manzello et al., 2015).

Understanding how coral calcification responds to rapid changes in seawater nutrient conditions and Ω_{sw} is critical for more accurate predictions of the persistence of reef habitats under the influence of global change. Tropical upwelling areas are well suited for this kind of research as the upwelling deep water masses are rich in nutrients and low in Ω_{sw}. This allows these regions to serve as natural laboratories to investigate the calcification response of reef corals to these multiple environmental stressors that are likely to affect global coral reefs in the near future (Camp et al., 2018; Wizemann et al., 2018). Published calcification data of the major reef-building coral *Porites* spp. growing within regions affected by seasonal upwelling are generally sparse and only available from three Pacific reef sites (Manzello et al., 2014; Mollica et al., 2018).

In this study, we report the first calcification data (calcification rate, extension rate, skeletal bulk density) of six *Porites* coral specimens from the so far unexplored region of the northern Arabian Sea upwelling zone (Masirah Island, Oman). Three out of the six samples that were considered representative for the site under study were selected for further geochemical analysis (Li/Mg, Ba/Ca). This facilitated the establishment of a detailed sub-annual chronology yielding monthly resolved records of calcification. This approach allowed for an unprecedented comparison of sub-annual calcification performance between the upwelling and non-upwelling season. In this way, this study improves the general knowledge on seasonal and annual patterns of reef coral calcification under exposure to variable Ω_{sw} and nutrient concentrations, thereby contributing to more accurate predictions on the persistence of reef habitats under the influence of global change.

2 Material and methods

2.1 Arabian Sea climate and oceanography

The Arabian Sea is the northwestern part of the Indian Ocean between India and the Arabian Peninsula (Fig. 1). The regional climate of the Arabian Sea is characterised by a semi-annual alternation of the prevailing wind directions (Beal et al., 2013). During Northern Hemisphere summer, strong winds of the southwest monsoon cross the Arabian Sea in the direction of the low-pressure system above the Tibetan Plateau (Findlater, 1969). During winter, reversal of the atmospheric pressure system causes the northeast monsoon (Hastenrath and Greischar, 1991). Low wind speeds without preferred orientation typically occur during the two inter-monsoon seasons (spring intermonsoon, autumn intermonsoon) (Beal et al., 2013; Lee et al., 2000). Surface wind
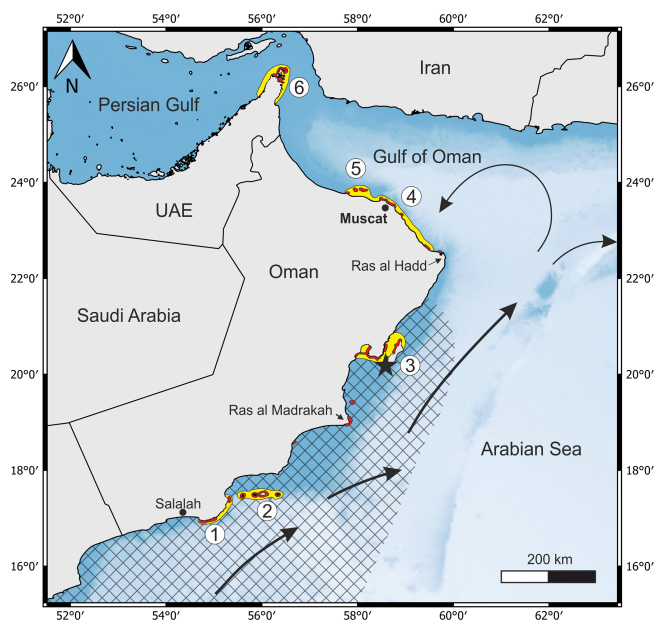
Figure 1. General map of the eastern Arabian Peninsula and the adjacent seas showing the reef sites (red) and coral reef provinces off Oman (yellow) (1 Marbat, 2 Kuria Muria Islands, 3 Masirah Island and Barr al Hikman, 4 capital area, 5 Daymaniyat Islands, and 6 Musandam; Salm, 1993; Burt et al., 2016). The black asterisk marks the sampling site at the southern tip of Masirah Island. Black arrows indicate the Omani current during the southwest monsoon. The hatched area delimitates the region of maximum upwelling inferred from August sea surface temperatures $< 25\,°C$ (1995–2005 monthly averages; WOA18, Locarnini et al., 2018). The blue shading displays water depth gradients (dark blue = shallow, light blue = deep).

fields are the driving force behind the upper hydrospheric structure and the seasonal variation in the oceanic surface current system (Swallow and Bruce, 1966). During summer, southwest monsoonal winds cause a strong coastal current (Oman Coastal Current), which runs northward parallel to the coast of the Arabian Peninsula and induces rigorous upwelling (Currie et al., 1973; Currie, 1992; Smith and Bottero, 1977). Increased nutrient supply during southwest monsoonal upwelling is associated with an increased primary productivity in the euphotic zone (Anderson et al., 1992; Bauer et al., 1991; Quinn and Johnson, 1996) (Fig. 2). Compared to equatorial upwelling regions of the eastern Pacific, the northern Arabian Sea upwelling is characterised by a high phosphate to nitrate ratio (Kleypas et al., 1999). But although nutrient supply is linked to upwelling, concentrations of PO_4^{3-} and NO_3^- remain at a high level throughout the year because of a prevailing iron limitation of the primary production (Mother Nature's iron experiment in Smith, 2001). Southwest monsoonal upwelling furthermore causes a drop in surface water pH, causing seawater aragonite saturation (Ω_{sw}) to decrease temporally from 3.5–4 during non-upwelling season to 3 during the upwelling season, which is

well below critical values assumed to be required for coral growth (i.e. $\Omega_{sw} > 3.3$) (Kleypas et al., 1999; Omer, 2010; Takahashi et al., 2014) (Fig. 2).

2.2 Coral growth and sample collection at Masirah Island

Coral growth off Oman occurs within six distinct provinces, including Marbat, the Kuria Muria Islands, Masirah Island and Barr al Hikman, the capital area, the Daymaniyat Islands, and Musandam (Fig. 1; Burt et al., 2016; Salm, 1993). The occurrence of corals at Masirah Island is limited to very shallow water depths of 1–4 m (Glynn, 1993). Fast growing cabbage and brain corals such as *Montipora* and *Platygyra* are the dominant genera, but massive *Porites* are also present (Coles, 1996).

In March 2018, dead coral material from six massive *Porites* colonies (sample identifier: 5.9; 5.10; 5.13; 5.15; 5.21; 5.22) was collected at the southernmost tip of Masirah Island from the uppermost part of the shore ($20.16°$ N, $58.64°$ E) (Fig. 1). This coral occurrence represents a storm deposit related to cyclone Gonu in 2007 (Fritz et al., 2010).

2.3 Methodology

Coral samples were cut to slices of 6 mm thickness parallel to the axis of maximum growth using a rock saw at lowest rotation speed and equipped with a water-cooled diamond blade. Subsequent usage of a CNC mill ensured coplanarity with maximum deviations of 1 %–3 % over the entire slab. The slabs were ultrasonically cleaned in deionised water and dried at $40\,°C$. Coral slabs were X-rayed using a digital X-ray cabinet (SHR 50 V) to document alternating growth bands of high (HDBs) and low density (LDBs) (Knutson et al., 1972), biogenic borings, encrustations, and cementation. Sampling transects for all further analyses were carefully selected so as not to be affected by bioerosion and encrustations but normal to HDBs and LDBs following trajectories of maximum linear extension (for the positioning of individual sampling transects see Fig. S1 in the Supplement). Density measurements were performed using X-ray densitometry based on CoralXDS software (Helmle et al., 2002, 2011). Greyscale-density calibrations were verified by measurements of standards for zero density (air, $\rho = 0\,g\,cm^{-3}$) and massive aragonite (*Tridacna* shell, $\rho = 2.93\,g\,cm^{-3}$) having the same thickness as the coral slabs. Maximum target deviations were $0.02 \pm 0.01\,g\,cm^{-3}$ for zero density (air) and $0.03 \pm 0.06\,g\,cm^{-3}$ for massive aragonite (*Tridacna* shell). The width of density measurement transects was set to 4 mm, including a representative mixture of approximately 12 corallites ($4\,mm \times 6\,mm$). Annual extension rates were estimated from the distance between two HDBs of maximum greyscale intensity on the radiographs. The mean annual skeletal density was calculated from the mean of all individual measure-
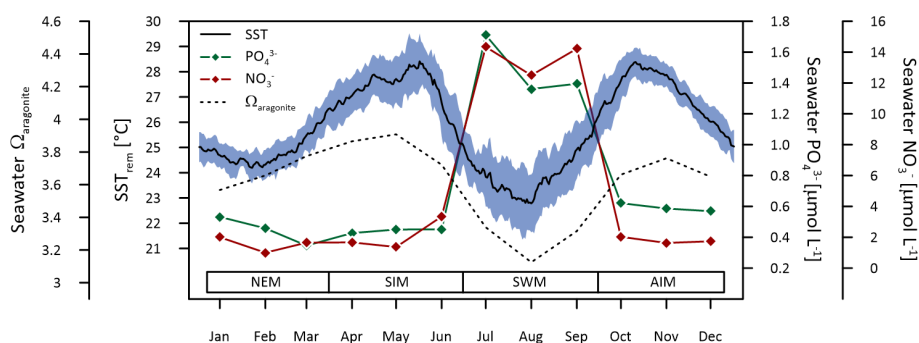
Figure 2. Ocean climatological data estimated from daily SSTs (JPL MUR MEaSUREs Project, 2015), monthly seawater phosphate (PO_4^{3-}) and nitrate (NO_3^-) concentrations (WOA18; Garcia et al., 2019), and aragonite saturation state ($\Omega_{aragonite}$) (Takahashi et al., 2014) at the sampling site. The blue shaded area represents the deviation (1σ) from averages of daily SSTs within the period 2003–2018. Seasonal abbreviations: NEM (northeast monsoon), SIM (spring intermonsoon), SWM (southwest monsoon), AIM (autumn intermonsoon).

ments along the transect and within one annual growth increment.

Corals 5.10, 5.13 and 5.21 were selected for Li/Mg and Ba/Ca geochemical analysis based on optimal orientation and traceability of the corallites adjacent to the density measurement transects (Fig. S1). Element concentrations were determined at the Institute for Geosciences, Johannes Gutenberg University Mainz (Germany), using an Agilent 7500ce inductively coupled plasma mass spectrometer (ICP-MS) coupled to an ESI NWR193 ArF excimer laser ablation (LA) system equipped with a TwoVol2 ablation cell. The ArF LA system was operated at a pulse repetition rate of 10 Hz and an energy density of ca. $3\,J\,cm^{-2}$. Ablation was carried out under a He atmosphere, and the sample gas was mixed with Ar before entering the plasma. Measurement spots with a beam diameter of 120 µm were aligned along transects in spot mode with a midpoint distance of 250 µm following discrete skeletal elements. Backgrounds were measured for 15 s prior to each ablation. Ablation time was 30 s, followed by 20 s of wash out. The isotopes monitored were ^{7}Li, ^{25}Mg, ^{43}Ca and ^{138}Ba. Signals were monitored in time-resolved mode and processed using an in-house Excel spreadsheet (Jochum et al., 2007). Details of the calculations are given in Mischel et al. (2017). NIST SRM 610 and SRM 612 were used as calibration material, applying the reference values reported in the GeoReM database (http://georem.mpch-mainz.gwdg.de/, last access: 26 July 2022, Application Version 27; Jochum et al., 2005, 2011) to calculate the element concentrations of the sample measurements. During each run, basaltic USGS BCR-2G, synthetic carbonate USGS MACS-3 and a nano-powder pellet of biogenic carbonate JCp-1 (Garbe-Schönberg and Müller, 2014) were analysed repeatedly as quality control materials (QCMs) to monitor precision and accuracy of the measurements and calibration strategy. All reference materials were analysed at the beginning and at the end of a sequence and after ca. 40 spots on the samples. For all materials ^{43}Ca was used as the internal standard, applying for the USGS BCR-2G and MACS-3 the pre-

ferred values reported in the GeoReM database: for JCp-1 38.18 wt % (Okai et al., 2002) and for the samples a Ca content of 39 wt % (Mertz-Kraus et al., 2009). Resulting element concentrations for the QCMs together with reference values are provided in the Supplement (Table S1). Element concentrations for the samples are converted into molar ratios of Ca, i.e. Li/Ca, Mg/Ca, Ba/Ca and Li/Mg.

Li/Mg thermometry was used for estimating absolute growth temperatures (Montagna et al., 2014; Cuny-Guirriec et al., 2019; Ross et al., 2019b; Hathorne et al., 2013; Fowell et al., 2016; D'Olivo et al., 2018; Zinke et al., 2019). The relationships between Li/Mg and SST have shown to be site dependent, however, and similar Li/Mg ratios produce differences in SST estimations of ∼ 2 °C between interreef (Hathorne et al., 2013) and intra-reef settings (Fowell et al., 2016). Such spatial variability in Li/Mg–SST relationships is likely due to poorly constrained effects of extension rate and seawater pH on skeletal Li/Mg ratios (Fowell et al., 2016; Fowell, 2017; Inoue et al., 2007; Tanaka et al., 2015). For this reason, we use a separate calibration of the Li/Mg thermometer for Masirah Island corals in order to overcome misleading SST estimates resulting from local seawater pH and extension rate effects associated with upwelling.

Ba/Ca ratios were used to identify skeletal portions calcified under upwelling conditions (Lea et al., 1989; Tudhope et al., 1996). Elevated Ba/Ca ratios in coral skeletons reflect high seawater Ba concentrations associated with upwelling deep waters, which are also nutrient-rich and acidic (Fallon et al., 1999; Montaggioni et al., 2006).

Daily sea surface temperatures (SST_{rem}) were extracted from JPL MUR (v4.1) available from https://podaac.jpl.nasa.gov (last access: 26 July 2022). The JPL MUR data range used for this study covers the period 2003–2018 and has a spatial resolution of 0.01° (grid cell: 19.90° N, 58.60° E). SSTs of equal calendar dates of consecutive years were averaged receiving one generalised annual record of mean daily SSTs for the period 2003–2018 (Fig. 2). Reliability of the remotely sensed data was confirmed by daily in situ

observed SSTs ($SST_{in\text{-}situ}$) recorded at the southern tip of Masirah Island (water depth: 5 m) between October 2001 and September 2002 (Wilson, 2007). Annual mean SSTs were in excellent agreement with each other ($SST_{rem} = 25.79\,°C$; $SST_{in\text{-}situ} = 25.54\,°C$), and daily SSTs were strongly correlated ($r^2 = 0.79$, $p < 0.0001$).

Monthly seawater phosphate and nitrate concentrations come from the World Ocean Atlas 2018 (WOA18) available on https://www.nodc.noaa.gov/OC5/woa18/woa18data.html (last access: 26 July 2022; grid cell: 19.5° N, 58.5° E, water depth: 5 m; Fig. 2). The WOA18 nutrient data are a generalised interpolation of all available in situ observations performed within individual months at certain depth levels within each 1° square (Garcia et al., 2019).

Monthly interpolated seawater aragonite saturation states for the northern Arabian Sea (Grid cell: 16.0° N, 57.5° E; Fig. 2) were extracted from https://www.ldeo.columbia.edu/res/pi/CO2/carbondioxide/pages/global_ph.html (last access: 26 July 2022; Takahashi et al., 2014).

2.4 Data matching and age model development

Records of skeletal density and element concentrations of corals 5.10, 5.13 and 5.21 were matched with optical microscope images allowing for the correlation of ablated spots from LA-ICP-MS with distinctive features on X radiographs. Slight offsets between the x axis of the LA-ICP-MS record and the density records can occur because to some extent the LA-ICP-MS sampling paths were not ultimately straight due to following discrete corallites and avoiding bioerosion traces and encrustations. To overcome this, the chronologies of the density records inferred from straight transects orientated parallel to the direction of growth were applied to the LA-ICP-MS records using AnalySeries software (Paillard et al., 1996).

Age models are based on Li/Mg ratios in combination with Ba/Ca ratios. Li/Mg is inversely related to temperature, which allows us to identify the two warm (intermonsoon) and two cool (monsoon) seasons (Hathorne et al., 2013). In order to identify the upwelling season among the two cool monsoon seasons (southwest monsoon, northeast monsoon), we use Ba/Ca ratios as proxy (Tudhope et al., 1996) (Fig. 3). A detailed chronological frame for the Li/Mg records was established with the aid of the generalised annual record of remote sensing SST data (JPL MUR, daily averaged 2003–2018) (Fig. 2). Dates of seasonal SST extremes, as well as dates of inflection points between consecutive seasons, were assigned to corresponding data points of the Li/Mg records (see Fig. S2 in the Supplement). This methodology allows us to tune the age models to a total of eight tie points per year (two per season). Dates between tie points were interpolated linearly, and the entire time axis was resampled to monthly intervals using AnalySeries software (Paillard et al., 1996). Accuracy of the age model was checked by comparing the timing of seasonal remote sensing SST maxima and

minima of individual years with dates of the generalised annual record (daily averages 2003–2018) and was found to be ± 4 weeks during the northeast monsoon, ± 3 weeks during the spring intermonsoon and southwest monsoon, and ± 1.5 weeks during the autumn intermonsoon.

3 Results

3.1 Coral Ba/Ca and Li/Mg records

Multi-year monthly means of the Ba/Ca records show pronounced maxima within one annual cycle, which have been used in establishing the age model to determine the southwest monsoonal upwelling season (Fig. 3) (Tudhope et al., 1996; Lea at al., 1989). Peak intensities vary considerably between samples, with coral 5.13 showing the lowest and coral 5.21 the highest Ba/Ca ratios during upwelling. All individual Ba/Ca records are positively related with WOA18 seawater phosphate and nitrate data (5.10: $r^2\,(PO_4^{3-}) = 0.68$, $p = 0.0009$, $r^2\,(NO_3^-) = 0.74$, $p = 0.0003$; 5.13: $r^2\,(PO_4^{3-}) = 0.84$, $p < 0.0001$, $r^2\,(NO_3^-) = 0.94$, $p < 0.0001$; 5.21: $r^2\,(PO_4^{3-}) = 0.77$, $p = 0.0002$, $r^2\,(NO_3^-) = 0.84$, $p < 0.0001$) (Garcia et al., 2019).

All multi-year monthly means of the Li/Mg records show pronounced patterns of two maxima and two minima within one annual cycle (Fig. 3). Li/Mg maxima coincide with peaks in Ba/Ca during southwest monsoonal upwelling, while a second maximum of Li/Mg is reached during winter. Minima occur during the intermonsoon seasons. All individual Li/Mg records exhibit the typical inverse relationship with monthly remote sensing SST data (JPL MUR) (5.10: $r^2 = 0.65$, $p = 0.0016$; 5.13: $r^2 = 0.75$, $p = 0.0003$; 5.21: $r^2 = 0.91$, $p < 0.0001$).

Multi-coral monthly means in Li/Mg are used for the calibration of the Li/Mg thermometer with mean monthly $SSTs_{rem}$ (averages of 2003–2018, JPL MUR) (Fig. 4). A total of 83 % of the intra-annual multi-coral monthly Li/Mg variation is explained by temperature, and the resultant SST calibration is estimated as

$$\text{Li/Mg [mmol mol}^{-1}] = -0.083(\pm 0.012) \times \text{SST} + 4.029(\pm 0.305)$$

$$(r^2 = 0.83;\ p < 0.0001). \tag{1}$$

3.2 Pattern of calcification

Mean annual skeletal density, extension rate and calcification rate, as well as the number of record years investigated within each of the six individual coral specimens, are shown in Table 2. Sub-annually resolved patterns of calcification of corals 5.10, 5.13 and 5.21 are expressed as multi-year monthly means (Fig. 5). The variability in monthly calcification rates within all three specimens is strongly determined by extension rates (5.10: $r^2 = 0.94$, $p < 0.0001$; 5.13:
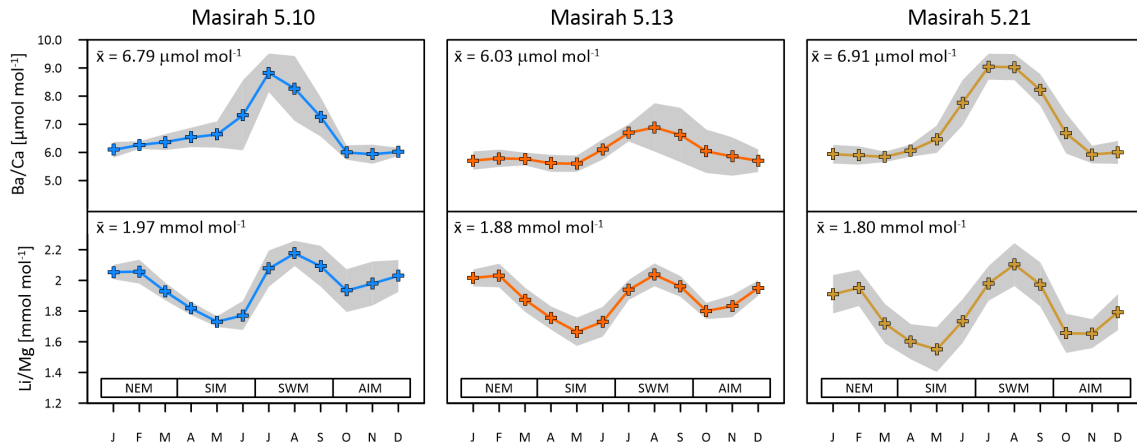
Figure 3. Multi-year monthly means in Ba/Ca and Li/Mg of three Masirah corals (blue, orange, yellow). The grey shaded area represents uncertainty (1σ) between equal months of consecutive years. Seasonal abbreviations: NEM (northeast monsoon), SIM (spring intermonsoon), SWM (southwest monsoon), AIM (autumn intermonsoon).
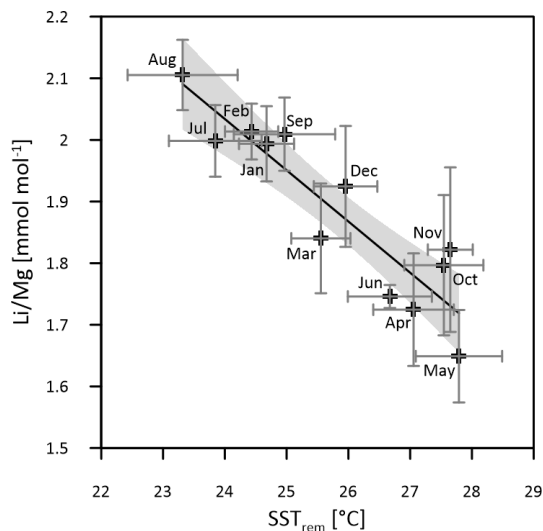
Figure 4. Multi-coral calibration of the Li/Mg thermometer with SSTs$_{rem}$ (monthly means 2003–2018, JPL MUR). Horizontal error bars (1σ) represent SST uncertainty between equal months of consecutive years (2003–2018), and vertical error bars (1σ) represent uncertainty of multi-year monthly mean Li/Mg ratios between the three Masirah corals. The grey shaded area indicates the 95% confidence interval of the linear regression.

Table 1. Mean seasonal SSTs ($\pm 1\sigma$) inferred from multi-year monthly mean Li/Mg ratios of individual corals from Masirah Island. Uncertainty (1σ) represents variability between equal seasons of consecutive years. Seasonal abbreviations: NEM (northeast monsoon), SIM (spring intermonsoon), SWM (southwest monsoon), AIM (autumn intermonsoon).

	5.10 Li/Mg–SST [°C]	5.13 Li/Mg–SST [°C]	5.21 Li/Mg–SST [°C]
SIM	27.03 ± 0.45	27.85 ± 0.88	29.00 ± 1.25
SWM	23.03 ± 0.95	24.79 ± 0.74	24.36 ± 1.25
AIM	25.00 ± 1.28	26.08 ± 0.48	28.49 ± 0.80
NEM	24.13 ± 0.42	24.88 ± 0.57	25.72 ± 1.19

$r^2 = 0.77$, $p < 0.0002$; 5.21: $r^2 = 0.81$, $p < 0.0001$). Corals 5.13 and 5.21 show three distinct peaks of highest extension rates in March, June and October. Reduced linear growth occurs during the southwest monsoon and northeast monsoon, as well as between April and May. Coral 5.10 slightly deviates from the pattern of the two other specimens by a lower growth rate during June, leading to two peaks of maximum extension in February/March and October. In this specimen, a decrease in linear growth starts in the spring intermonsoon and reaches its minimum during the southwest monsoon.

Sub-annual variability in skeletal bulk density of coral specimens 5.10 and 5.13 shows a pattern of two distinct high-density bands (HDBs) between two bands of low density (LDB) within one annual growth increment (Fig. 5). Skeletal portions of low density were deposited during the spring intermonsoon and autumn intermonsoon, and high-density portions formed during the southwest monsoon and northwest monsoon. This alternating pattern of HDBs and LDBs causes skeletal density variation in corals 5.10 and 5.13 to be significantly inversely related to monthly reconstructed Li/Mg and SSTs (5.10: $r^2 = 0.87$, $p < 0.0001$; 5.13: $r^2 = 0.34$, $p < 0.05$) (Fig. 6c). This is not the case for coral 5.21, as a well-expressed LDB equivalent with the autumn intermonsoon is lacking. Rather, it shows one wide LDB with density increasing from the southwest monsoon to northeast monsoon.

Calcification rates during the southwest monsoon are only 51%, 96% and 78% of those observed during the northwest monsoon (for corals 5.10, 5.13 and 5.21, respectively) (Table 3; Fig. 6a). These differences in seasonal
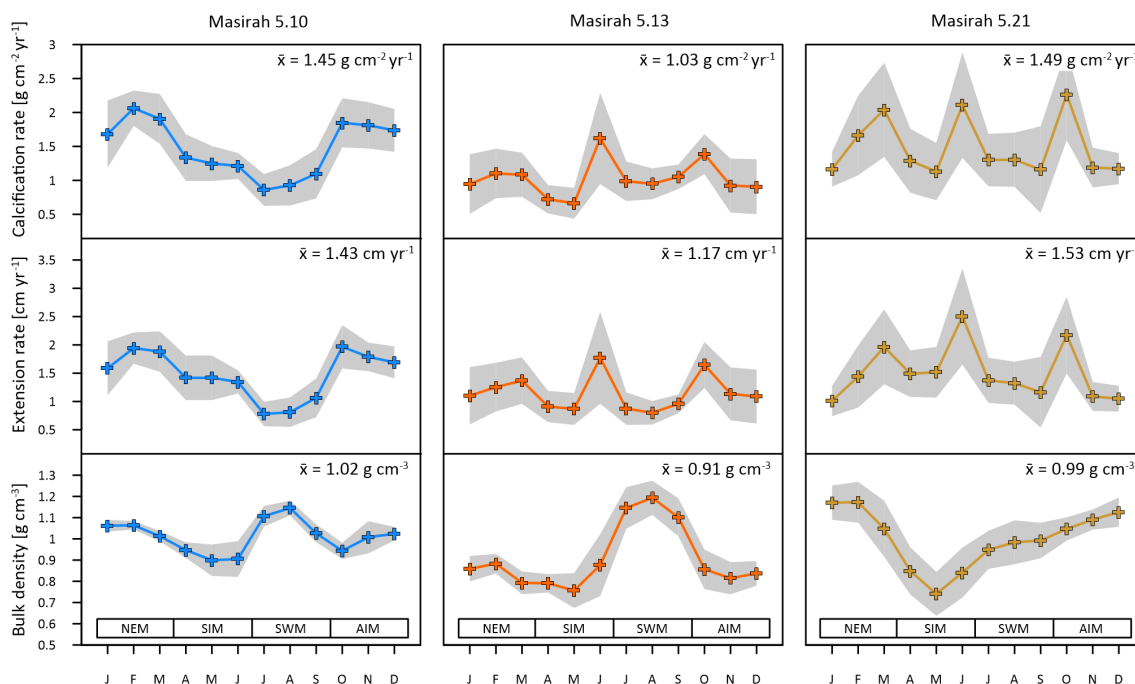
Figure 5. Results of multi-year monthly means of calcification rate, extension rate and skeletal density of three corals from Masirah Island (blue, orange, yellow). The grey shaded area represents uncertainty (1σ) between equal months of consecutive years. Seasonal abbreviations: NEM (northeast monsoon), SIM (spring intermonsoon), SWM (southwest monsoon), AIM (autumn intermonsoon).

Table 2. Mean annual skeletal bulk density, linear extension rate and calcification rate ($\pm 1\sigma$) of all six coral specimens from Masirah Island. Uncertainty (1σ) represents variability between consecutive record years.

|	Record years [n]	Bulk density [$\mathrm{g\,cm^{-3}}$]	Extension rate [$\mathrm{cm\,yr^{-1}}$]	Calcification rate [$\mathrm{g\,cm^{-2}\,yr^{-1}}$]
5.9	6	1.03 ± 0.04	1.19 ± 0.16	1.22 ± 0.15
5.10	3	1.02 ± 0.02	1.43 ± 0.05	1.45 ± 0.08
5.13	5	0.91 ± 0.06	1.17 ± 0.12	1.03 ± 0.07
5.15	3	1.07 ± 0.04	1.07 ± 0.16	1.14 ± 0.14
5.21	5	0.99 ± 0.07	1.53 ± 0.11	1.49 ± 0.10
5.22	4	0.95 ± 0.05	1.47 ± 0.13	1.38 ± 0.08

calcification rates are related to low extension rates during southwest monsoonal upwelling, which are 49 %, 71 % and 91 % relative to those observed during the northeast monsoon (for corals 5.10, 5.13 and 5.21, respectively). Interestingly, monthly extension rates during the southwest monsoon exhibit a strong negative correlation with skeletal density patterns across all three specimens ($r^2 = 0.88$, $p = 0.0002$), which is not the case during the northeast monsoon ($r^2 = 0.04$, $p = 0.60$) (Fig. 7). According to individual extension rates during the southwest monsoon, this produces varying density patterns across the three specimens, with corals 5.13 and 5.10 having the lowest extension rate during the southwest monsoon and showing the highest intra-annual skeletal density during this season (Table 3; Fig. 5). Coral 5.21 that shows relatively fast extension growth dur-

ing the southwest monsoon compared to all other specimens only reveals a moderate increase in skeletal density, which remains below those observed during the northeast monsoon.

4 Discussion

4.1 Ba/Ca records

Multi-year monthly means in skeletal Ba/Ca are in excellent agreement with WOA18 nutrient data. This confirms Ba/Ca to be an appropriate proxy for intra-annual variability in seawater nutrient concentrations (Fallon et al., 1999; Montaggioni et al., 2006). Effects of riverine input on the skeletal Ba/Ca record can be excluded due to the absence of rivers in the arid region of northeastern Oman (Alibert et al., 2003;
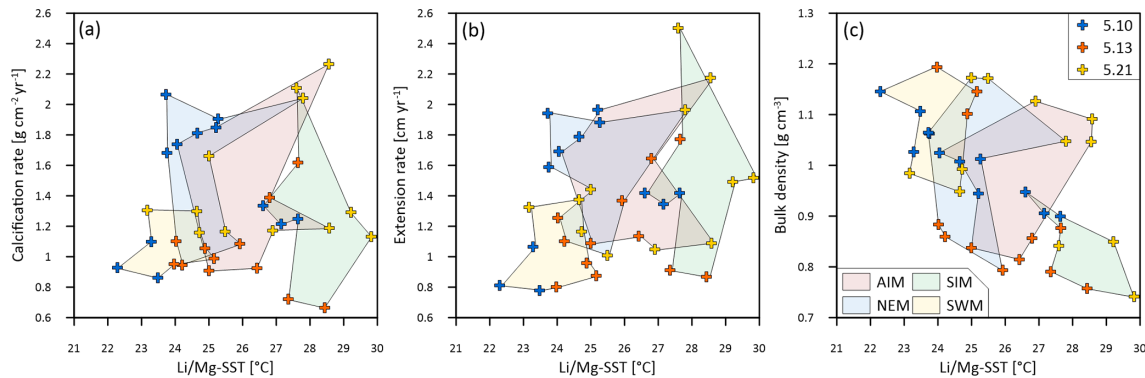
Figure 6. Multi-year monthly means of **(a)** calcification rate, **(b)** extension rate and **(c)** skeletal bulk density and associated Li/Mg and SSTs of three corals from Masirah Island (blue, orange, yellow). The coloured shaded polygons combine monthly data that belong to the same season. Seasonal abbreviations: NEM (northeast monsoon), SIM (spring intermonsoon), SWM (southwest monsoon), AIM (autumn intermonsoon).

Table 3. Mean seasonal skeletal bulk density, linear extension rate and calcification rate ($\pm 1\sigma$) of three corals from Masirah Island. Uncertainty (1σ) represents variability between equal seasons of consecutive years. Seasonal abbreviations: NEM (northeast monsoon), SIM (spring intermonsoon), SWM (southwest monsoon), AIM (autumn intermonsoon).

	5.10			5.13			5.21		
	Bulk density [$\mathrm{g\,cm^{-3}}$]	Extension rate [$\mathrm{cm\,yr^{-1}}$]	Calcification rate [$\mathrm{g\,cm^{-2}\,yr^{-1}}$]	Bulk density [$\mathrm{g\,cm^{-3}}$]	Extension rate [$\mathrm{cm\,yr^{-1}}$]	Calcification rate [$\mathrm{g\,cm^{-2}\,yr^{-1}}$]	Bulk density [$\mathrm{g\,cm^{-3}}$]	Extension rate [$\mathrm{cm\,yr^{-1}}$]	Calcification rate [$\mathrm{g\,cm^{-2}\,yr^{-1}}$]
SIM	0.94 ± 0.04	1.26 ± 0.23	1.18 ± 0.20	0.81 ± 0.07	1.25 ± 0.34	1.02 ± 0.25	0.80 ± 0.1	1.83 ± 0.30	1.47 ± 0.33
SWM	1.10 ± 0.01	0.87 ± 0.06	0.95 ± 0.06	1.15 ± 0.08	0.90 ± 0.18	1.02 ± 0.18	0.94 ± 0.05	1.31 ± 0.23	1.24 ± 0.28
AIM	0.99 ± 0.03	1.83 ± 0.28	1.81 ± 0.33	0.83 ± 0.07	1.25 ± 0.27	1.03 ± 0.21	1.09 ± 0.06	1.55 ± 0.20	1.65 ± 0.19
NEM	1.05 ± 0.01	1.79 ± 0.17	1.88 ± 0.17	0.85 ± 0.05	1.26 ± 0.31	1.06 ± 0.26	1.12 ± 0.1	1.44 ± 0.20	1.58 ± 0.11
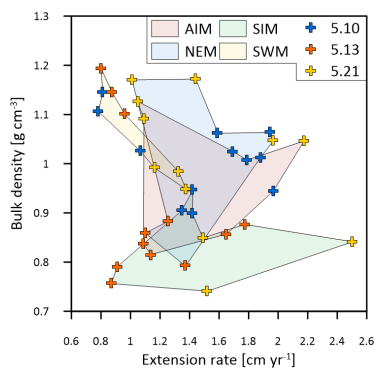
Figure 7. Multi-year monthly means in extension rate versus skeletal bulk density of the three corals from Masirah Island (blue, orange, yellow). The coloured shaded polygons combine monthly data that belong to the same season. Seasonal abbreviations: NEM (northeast monsoon), SIM (spring intermonsoon), SWM (southwest monsoon), AIM (autumn intermonsoon).
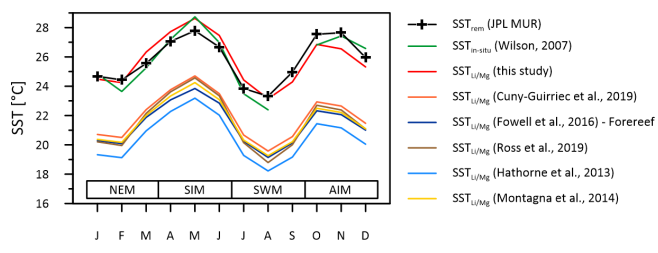
Figure 8. Instrumental SSTs (green line) compared to multi-coral monthly mean SSTs inferred from Li/Mg ratios of the Masirah corals using the calibration of this study (red line) and calibrations reported from the literature. Published Li/Mg–SST calibrations cause variable degrees of underestimation of reconstructed SST at Masirah Island. Seasonal abbreviations: NEM (northeast monsoon), SIM (spring intermonsoon), SWM (southwest monsoon), AIM (autumn intermonsoon).

Jiang et al., 2017). This allows intra-annual variability in Ba/Ca to be fully attributed to upwelling (Tudhope et al., 1996; Lea et al., 1989). Variable Ba/Ca ratios across specimens during the southwest monsoonal upwelling season are likely to result from spatial heterogeneous seawater barium distribution within the reef.

4.2 Li/Mg records

SST reconstructions based upon the calibration of the Li/Mg thermometer described above (Eq. 1) reproduce the monthly curve of the $\mathrm{SST_{rem}}$ data ($r^2 = 0.83$, $p < 0.0001$), as well as observed $\mathrm{SST_{in\text{-}situ}}$ variations at Masirah Island ($r^2 = 0.93$, $p < 0.0001$) (Wilson, 2007). Temperature sensitivity of the Li/Mg thermometer deduced from reconstructed seasonal-

ity is in good agreement with the majority of proxy calibration studies from the literature (Hathorne et al., 2013; Ross et al., 2019b; Cuny-Guirriec et al., 2019; Montagna et al., 2014; Fowell et al., 2016). The intercept of the linear Li/Mg–SST calibration of the Masirah corals, however, is 4–5 °C higher than reported in the literature (Fig. 8). Analytical uncertainties that noticeably bias the Li/Mg ratio are unlikely to be a source for high Li/Mg ratios because systematic measurement discrepancies deduced from the JCp-1 QCM for Li/Ca and Mg/Ca would tend to underestimate the Li/Mg ratios (Li/Ca: +4.44 %; Mg/Ca: +7.37 %; Table S1). In addition to temperature, seawater pH also has been shown to bias the skeletal Li/Mg ratio of corals (Fowell et al., 2016; Fowell, 2017; Tanaka et al., 2015). For identical SSTs, culture experiments on *Siderastrea siderea* show an increase of $0.325\,\mathrm{mmol\,mol^{-1}}$ in Li/Mg per decreasing $\mathrm{pH_{sw}}$ unit (Fowell, 2017). However, comparatively high Li/Mg values found in the Masirah corals are present year-round, while exceptionally low $\mathrm{pH_{sw}}$ is limited to the 3-month southwest monsoon upwelling season (Omer, 2010; Takahashi et al., 2014). This suggests that skeletal Li/Mg is not directly sensitive to the external $\mathrm{pH_{sw}}$ but rather to the carbonate chemistry of the calcification fluid, which through modification is independent of external variations in $\mathrm{pH_{sw}}$ (McCulloch et al., 2017). Conditions within the calcifying fluid must permanently alter skeletal Li/Mg of *Porites* at Masirah Island towards higher values compared to published SST–Li/Mg calibrations reported in the literature, which might imply year-round stable but low $\mathrm{pH_{cf}}$.

4.3 Skeletal calcification

4.3.1 Monthly records of coral calcification

Monthly variability in calcification rates are largely driven by extension rates across all samples (Fig. 5), similar to that reported for *Porites* from the Indo-Pacific region (Lough and Barnes, 2000). However, the typical positive correlation between monthly extension rates and SST does not exist in our data (Fig. 6b). All three specimens reveal noticeably small extension growth during April and May despite high temperatures during the spring intermonsoon. Interestingly, coral spawning at Omani reef sites is reported to take place between March and May (Howells et al., 2014). Correspondingly, a reduction in extension rate during the spring intermonsoon could be linked to high-energy expenditures required for reproduction (Cabral-Tena et al., 2013).

All specimens show lower calcification rates during the southwest monsoon compared to those observed for the northeast monsoon, which is attributed to smaller extension rates during the upwelling (Table 3). The declining extension rate during the upwelling season is in agreement with growth studies on *Pocillopora damicornis* from the Gulf of Panama (Glynn, 1977). For corals from Masirah Island, at least part of the seasonal difference in extension rate between the southwest monsoon and northeast monsoon might be related to slightly lower SSTs during the southwest monsoonal upwelling (Table 1). Given an increase in extension rate of $0.33\,\mathrm{cm\,yr^{-1}}$ per 1 °C as suggested for Indo-Pacific *Porites*, differences in extension rates between the southwest monsoon and northeast monsoon could be fully explained by temperature for coral 5.21 but only to some extent for corals 5.10 and 5.13 (Lough and Barnes, 2000).

Intense eutrophication might have an additional impact on the growth of Masirah corals, with detrimental effects on extension rate during the upwelling season (Tomascik, 1990). Assuming direct detrimental effects of the essential nutrients on coral growth, the inhibiting effect of $\mathrm{NO_3^-}$ would have to outweigh the promoting effect of $\mathrm{PO_4^{3-}}$ on southwest monsoon extension rates of the Masirah corals (Koop et al., 2001; Dunn et al., 2012; Bucher and Harrison, 2001). However, the northern Arabian Sea is characterised by a high $\mathrm{PO_4^{3-}}$ to $\mathrm{NO_3^-}$ ratio, making this direct effect of nutrients on the extension rate unlikely (Kleypas et al., 1999). As a general consequence of the excessively high nutrient concentrations, primary productivity in the Arabian Sea increases rapidly during the upwelling season, leading to high levels of turbidity associated with low light transparency of the water column (Anderson et al., 1992; Bauer et al., 1991; Quinn and Johnson, 1996). Reduced photosynthetic efficiency of the micro-algae symbionts seems to be a potential factor for diminished extension rate in response to reduced energy reserves during upwelling (Al Shehhi et al., 2014; Logan and Tomascik, 1991; Muscatin et al., 1981; Sun et al., 2008; Tomascik, 1990). Energy through heterotrophic feeding does not seem to be sufficient for Masirah corals to fully compensate for reduced levels of photosynthates (Tomascik and Sander, 1985). Interestingly, the highest monthly extension rates occur immediately before and after the upwelling season during June and October, respectively (Fig. 5). A decrease in the extension growth during the southwest monsoon sets on immediately at the beginning of the upwelling, only to recover rapidly again afterwards. We therefore conclude that the coral's energy reserves available for skeletal upward growth respond instantaneously to monthly environmental changes (i.e. turbidity), without delays or extended times for recovery.

In contrast to *Porites* from the Indo-Pacific region, which show only a moderate dependence of skeletal density on SST, Li/Mg and SSTs at Masirah Island are strongly correlated with the monthly variation in skeletal density in corals 5.10 and 5.13 (Lough and Barnes, 2000). This is however not observed for coral 5.21, as a weakly developed HDB during the southwest monsoon weakens any relationship with SST (Fig. 6c). This comparatively low density during southwest monsoonal upwelling coincides with a relatively high extension rate in coral 5.21 compared to all other samples (Table 3; Fig. 6b). Excellent negative correlation between southwest monsoonal data of monthly density and extension rate
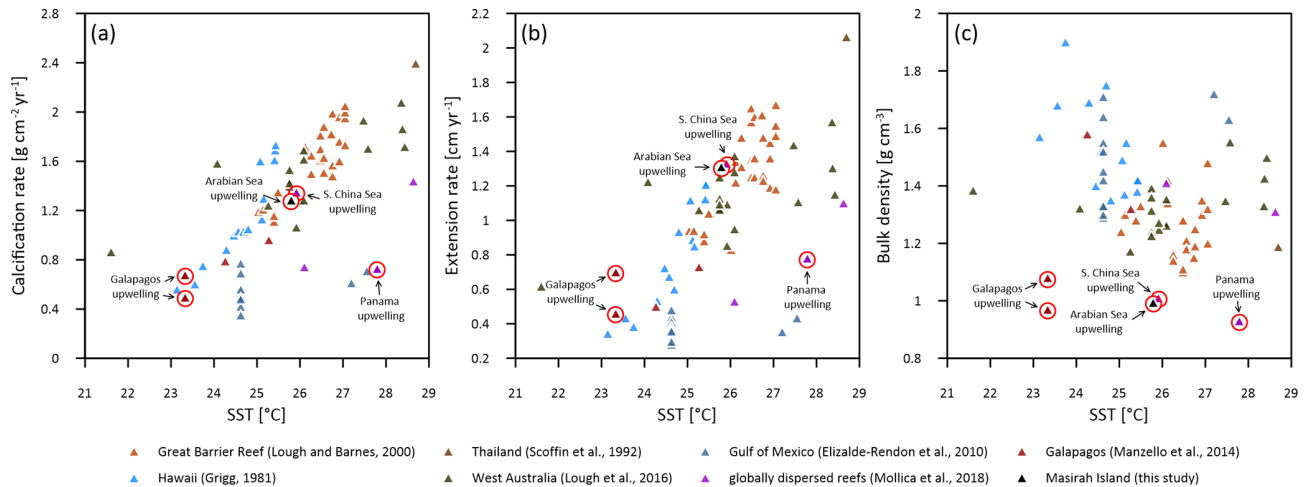
Figure 9. Annual means of *Porites* calcification rate (**a**), extension rate (**b**) and skeletal bulk density (**c**) versus sea surface temperature (SST) from various Indo-Pacific and western Atlantic reef sites. Red circles indicate sites affected by seasonal upwelling.

across the three corals ($n = 9$, $r^2 = 0.88$, $p = 0.0002$) indicates density during upwelling to be substantially controlled by extension rate (Fig. 7). A simple model in which the active calcification surface to which $CaCO_3$ is accreted is relatively large at high extension rate, resulting in thin skeletal elements and low bulk density (and vice versa for HDBs) might explain inter-specimen variability in skeletal density patterns of the Masirah corals during the southwest monsoon (DeCarlo and Cohen, 2017). No evidence supports an immediate detrimental impact of upwelling, i.e. a temporally low Ω_{sw}, on sub-annual patterns in skeletal density. Given that density is likely controlled by the carbonate chemistry of the calcification fluid, we propose Ω_{cf} is kept relatively constant by modification independent of external variations in Ω_{sw} during upwelling and non-upwelling seasons (DeCarlo et al., 2018; McCulloch et al., 2017; Mollica et al., 2018).

4.3.2 Annual records of coral calcification

The mean annual calcification rate at Masirah Island is indistinguishable from those of *Porites* from Indo-Pacific and Atlantic reef sites, which are unaffected by upwelling (Fig. 9a). A similar finding is reported from two sites located within the Galapagos upwelling zone ($n = 7$–8 cores per site) (Manzello et al., 2014). Poor replication of *Porites* calcification data from the upwelling areas of Panama and the South China Sea ($n = 1$, respectively) does not enable a proper comparison (Mollica et al., 2018). Patterns of calcification in *Porites* from Masirah Island and Galapagos differ from those found in regions without upwelling by showing enhanced extension rates and lower skeletal densities, similar to the pattern termed "stretching modulation of skeletal growth" by Carricart-Ganivet (2004) (Fig. 9b and c). The high mean annual *Porites* extension rate at Galapagos was discussed as a potential impact of the stimulating effects of nutri-

ents on upward growth (Manzello et al., 2014). Nutrient-stimulated growth is also suggested for enhanced annual extension growth of *Pocillopora damicornis* and *Pavona clavus* from the Panama upwelling zone compared to data from regions unaffected by upwelling (Glynn, 1977; Wellington and Glynn, 1983). In fact, the enhanced annual extension rate of *Pavona clavus* from Panama is the result of high extension growth during the non-upwelling season, similar to the pattern seen in *Porites* from Masirah Island (Wellington and Glynn, 1983) (Table 3). Hence, a stimulating effect of nutrients on extension rate during the non-upwelling seasons is possible since moderate nutrient concentrations with high PO_4^{3-} to NO_3^- ratio exist year-round in the Arabian Sea (Dunn et al., 2012; Kleypas et al., 1999; Koop et al., 2001).

The low skeletal density of coral specimens from Masirah Island is consistent with low skeletal density reported in the literature for *Porites* from the upwelling regions of the eastern Pacific and the China Sea (Mollica et al., 2018; Manzello et al., 2014) (Fig. 9c). Boron isotope analyses on some of these samples have revealed the low skeletal density to be driven by a relatively low Ω_{cf} compared to corals from regions unaffected by upwelling (Mollica et al., 2018). Low Ω_{cf} in these specimens is maintained year-round, independent of external variations in Ω_{sw} (i.e. seasonal upwelling) (Fig. S3 in the Supplement). Accordingly, we hypothesise the year-round relatively low skeletal density of the Masirah corals to be also related to a constantly low Ω_{cf}. This hypothesis is further supported by the Li/Mg ratios of the Masirah corals, which are offset to higher values than those expected from the literature (Fig. 8). As this offset is present throughout the year, it cannot be attributed to temporarily low pH_{sw} associated with seasonal upwelling but rather reflects year-round constant conditions within the calcifying fluid (Fowell, 2017; McCulloch et al., 2017). This finding implies that there is no intensified upregulation of internal Ω_{cf} relative to Ω_{sw}

during the non-upwelling seasons (McCulloch et al., 2017; DeCarlo et al., 2018; D'Olivo and McCulloch, 2017). As an explanation, we propose that internal upregulation processes of corals affected by seasonal upwelling are not capable to adapt completely to ocean chemistry change on a quarterly scale. As a consequence, a relatively low Ω_{cf} could be maintained year-round so as to avoid high gradients to the external Ω_{sw} during southwest monsoonal upwelling.

5 Conclusion

This study investigates the effect of seasonal upwelling on sub-annual and annual patterns of calcification in reef corals (*Porites*) from the northern Arabian Sea (Masirah Island, Oman). On a sub-annual basis, calcification rates are lower during the upwelling season compared to periods of near-identical SST in the non-upwelling season. This is attributed to a rapid decline in extension rates with the onset of the upwelling season. We attribute this decline to a reduction in photosynthetic performance of the micro-algae symbionts potentially caused by enhanced turbidity of ambient seawater through elevated primary production. Patterns of skeletal density do not exhibit an instantaneous response to the external decline in Ω_{sw} during upwelling, which indicates stable levels of Ω_{cf} being maintained throughout the year. Nonetheless, mean annual skeletal densities are significantly lower than in *Porites* from typical reef environments of the Indo-Pacific and Atlantic Ocean. In contrast, mean annual extension rates are high likely due to the simulating effect of moderate seawater nutrient concentrations during the non-upwelling seasons. As high extension growth compensates for the deficit in skeletal density at Masirah Island, annual calcification rates are indistinguishable from *Porites* growing in regions unaffected by upwelling.

These results suggest that temporarily reduced Ω_{sw} (seasonal upwelling) has no instantaneous impact on sub-annual variability in skeletal density but could cause a permanent adaptation towards year-round unexpected low skeletal density. Further research should include combined analyses of $\delta^{11}B$ and B/Ca ratios in order to confirm the hypothesis of the permanently low skeletal density in reef corals from sites affected by seasonal upwelling being controlled by a year-round comparatively low Ω_{cf}. Unless the low skeletal density is compensated through high extension rate, this will yield detrimental effects on the net carbonate accumulation in coral reefs. Furthermore, this study highlights variable effects of nutrients on extension rate, with negative effects at excessively high nutrient levels (i.e. upwelling season) and stimulatory effects at moderate nutrient levels (i.e. non-upwelling season).

Author contributions. PMS designed this research in close collaboration with TCB and MR. Field work was carried out by PMS, TCB and MR and substantially supported by OT. Laboratory analyses were performed by PMS and RMK. All authors had a contribution in writing and improving the manuscript.

References

Al-Rousan, S.: Skeletal extension rate of the reef building coral *Porites* species from Aqaba and their environmental variables, Natural Science, 4, 731–739, https://doi.org/10.4236/ns.2012.49097, 2012.

Al Shehhi, M. R., Gherboudj, I., and Ghedira, H.: An overview of historical harmful algae blooms outbreaks in the Arabian Seas, Mar. Pollut. Bull., 86, 314–324, https://doi.org/10.1016/j.marpolbul.2014.06.048, 2014.

Alibert, C., Kinsley, L., Fallon, S. J., McCulloch, M. T., Berkelmans, R., and McAllister, F.: Source of trace element variability in Great Barrier Reef corals affected by the Burdekin flood plumes, Geochim. Cosmochim. Ac., 67, 231–246, https://doi.org/10.1016/S0016-7037(02)01055-4, 2003.

Anderson, D. M., Brock, J. C., and Prell, W. L.: Physical upwelling process, upper ocean environment and the sediment record of the southwest monsoon. Upwelling systems: Evolution since the early Miocene, Geol. Soc. Spec. Publ., 64, 121–129, https://doi.org/10.1144/GSL.SP.1992.064.01.08, 1992.

Barott, K. T. and Rohwer, F. L.: Unseen players shape benthic competition on coral reefs, Trends Microbiol., 20, 621–628, https://doi.org/10.1016/j.tim.2012.08.004, 2012.

Bauer, S., Hitchcock, G. L., and Olson, D. B.: Influence of monsoonally-forced Ekman dynamics upon surface layer depth and plankton biomass distribution in the Arabian Sea, Deep-Sea Res., 38, 531–553, https://doi.org/10.1016/0198-0149(91)90062-K, 1991.

Beal, L. M., Hormann, V., Lumpkin, R., and Foltz, G. R.: The response of the surface circulation of the Arabian Sea to monsoonal forcing, J. Phys. Oceanogr., 43, 2008–2022, https://doi.org/10.1175/JPO-D-13-033.1, 2013.

Bucher, D. J. and Harrison, P. L.: Growth response of the reef coral *Acropora longicyathus* to elevated inorganic nutrients: do responses to nutrients vary among coral taxa?, Proceedings 9th International Coral Reef symposium, 23–27 October 2000, Bali, Indonesia, 443–448, 2001.

Burt, J. A., Coles, S., van Lavieren, H., Taylor, O., Looker, E., and Samimi-Namin, K.: Oman's coral reefs: A unique ecosystem challenged by natural and man-related stresses and in need of conservation, Mar. Pollut. Bull., 105, 498–506, https://doi.org/10.1016/j.marpolbul.2015.11.010, 2016.

Cabral-Tena, R. A., Reyes-Bonilla, H., Lluch-Cota, S., Paz-García, D. A., Calderón-Aguilera, L. E., Norzagaray-López, O., and Balart, E. F.: Different calcification rates in males and females of the coral *Porites panamensis* in the Gulf of California, Mar. Ecol. Prog. Ser., 476, 1–8, https://doi.org/10.3354/meps10269, 2013.

Camp, E. F., Schoepf, V., Mumby, P. J., Hardtke, L. A., Rodolfo-Metalpa, R., Smith, D. J., and Suggett, D. J.: The future of coral reefs subject to rapid climate change: Lessons from natural extreme environments, Front. Mar. Sci., 5, 1–21, https://doi.org/10.3389/fmars.2018.00004, 2018.

Cantin, N. E., Cohen, A. L., Karnauskas, K. B., Tarrant, A. M., and McCorkle, D. C.: Ocean warming slows coral growth in the central Red Sea, Science, 329, 322–325, https://doi.org/10.1126/science.1190182, 2010.

Carricart-Ganivet, J. P.: Sea surface temperature and the growth of the West Atlantic reef-building coral *Montastraea annularis*, J. Exp. Mar. Biol. Ecol., 302, 249–260, https://doi.org/10.1016/J.JEMBE.2003.10.015, 2004.

Carricart-Ganivet, J. P., Merino, M.: Growth responses of the reef-building coral *Montastraea annularis* along a gradient of continental influence in the southern Gulf of Mexico, B. Mar. Sci., 68, 133–146, 2001.

Chen, M., Martin, P., Goodkin, N. F., Tanzil, J., Murty, S., and Wiguna, A. A.: An assessment of P specification and P : Ca proxy calibration in coral cores from Singapore and Bali, Geochim. Cosmochim. Ac., 267, 113–123, https://doi.org/10.17632/2hbxk2njfx.1, 2019.

Chen, T. and Yu, K.: P/Ca in coral skeleton as a geochemical proxy for seawater phosphorus variation in Daya Bay, northern South China Sea, Mar. Pollut. Bull., 62, 2114–2121, https://doi.org/10.1016/j.marpolbul.2011.07.014, 2011.

Coles, S. L.: Corals of Oman. R.Keech, Thornes, Hawes, North Yorkshire, 106 pp., 1996.

Cornwall, C. E., Comeau, S., Kornder, N. A., Perry, C. T., van Hooidonk, R., DeCarlo, T. M., Pratchett, M. S., Anderson, K. D., Browne, N., Carpenter, R., Diaz-Pulido, G., D'Olivo, J. P., Doo, S. S., Figueiredo, J., Fortunato, S. A. V., Kennedy, E., Lantz, C. A., McCulloch, M. T., González-Rivero, M., Schoepf, V., Smithers, S. G., and Lowe, R. J.: Global declines in coral reef calcium carbonate production under ocean acidification and warming, P. Natl. Acad. Sci. USA, 118, e20152651, https://doi.org/10.1073/pnas.2015265118, 2021.

Cuny-Guirriec, K., Doouville, E., Reynaud, S., Allemand, D., Bordier, L., Canesi, M., Mazzoli, C., Taviani, M., Canese, S., McCulloch, M., Trotter, J., Rico-Esenaro, S. D., Sanchez-Cabeza, J. A., Ruiz-Fernández, A. C., Carricart-Garnivet, J. P., Scott, P. M., Sadekov, A., and Montagna, P.: Coral Li/Mg thermometry: Caveats and constrains, Chem. Geol., 532, 162–178, https://doi.org/10.1016/j.chemgeo.2019.03.038, 2019.

Currie, R. I.: Circulation and upwelling off the coast of South-East Arabia, Oceanol. Acta, 15, 43–60, 1992.

Currie, R. I., Fisher A. E., and Hargreaves P. M.: Arabian Sea Upwelling, in: The Biology of the Indian Ocean. Ecological Studies (Analysis and Synthesis), vol. 3., edited by: Zeitzschel B. and Gerlach S. A., Springer, Berlin, Heidelberg, https://doi.org/10.1007/978-3-642-65468-8, 1973.

D'Olivo, J. P. and McCulloch, M.: Response of coral calcification and calcifying fluid composition to thermally induced bleaching stress, Sci. Rep., 7, 1–15, https://doi.org/10.1038/s41598-017-02306-x, 2017.

D'Olivo, J. P., McCulloch, M. T., and Judd, K.: Long-term records of coral calcification across the central Great Barrier Reef: assessing the impact of river runoff and climate change, Coral Reefs, 32, 999–1012, https://doi.org/10.1007/s00338-013-1071-8, 2013.

D'Olivo, J. P., Sinclair, D. J., Rankenburg, K., and McCulloch, M. T.: A universal multi-trace element calibration for reconstructing sea surface temperatures from long-lived Porites corals: Removing "vital effects", Geochim. Cosmochim. Ac., 239, 109–135, https://doi.org/10.1016/j.gca.2018.07.035, 2018.

D'Olivo, J. P., Ellwood, G., DeCarlo, T. M., and McCulloch, M. T.: Deconvolving the long-term impacts of ocean acidification and warming on coral biomineralisation, Earth Planet. Sc. Lett., 526, 115785, https://doi.org/10.1016/j.epsl.2019.115785, 2019.

DeCarlo, T. M. and Cohen, A. L.: Dissipiment, density bands and signatures of thermal stress in *Porites* skeletons, Coral Reefs, 36, 749–761, https://doi.org/10.1007/s00338-017-1566-9, 2017.

DeCarlo, T. M., Comeau, S., Cornwall, C. E., and McCulloch, M. T.: Coral resistance to ocean acidification linked to increased calcium at the site of calcification, P. Roy. Soc. B-Biol. Sci., 285, 1–7, https://doi.org/10.1098/rspb.2018.0564, 2018.

Dodge, R. E. and Brass, G. W.: Skeletal extension, density and calcification of the reef coral, *Montastrea annularis*: St. Croix, U. S. Virgin Islands, B. Mar. Sci., 34, 288–307, 1984.

Dunn, J. G., Sammarco, P. W., and LaFleur Jr, G.: Effects of phosphate on growth and skeletal density in the

scleractinian coral *Acropora muricata*: A controlled experimental approach, J. Exp. Mar. Biol. Ecol., 411, 34–44, https://doi.org/10.1016/j.jembe.2011.10.013, 2012.

Elizalde-Rendón, E. M., Horta-Puga, G., González-Diaz, P., and Carricart-Ganivet, J. P.: Growth characteristics of the reef-building coral *Porites astreoides* under different environmental conditions in the Western Atlantic, Coral Reefs, 29, 607–614, https://doi.org/10.1007/s00338-010-0604-7, 2010.

Fallon, S. J., McCulloch, M. T., Van Woesik, R., and Sinclair, D. J.: Corals at their latitudinal limits: Laser ablation trace element systematics in *Porites* from Shirigai Bay, Japan, Earth Planet. Sc. Lett., 172, 221–238, https://doi.org/10.1016/S0012-821X(99)00200-9, 1999.

Findlater, J.: A major low-level air current near the Indian Ocean during the northern summer, Q. J. Roy. Meteor. Soc., 95, 362–380, https://doi.org/10.1002/qj.49709540409, 1969.

Fowell, S. E.: Assessing the magnitude of anthropogenic ocean warming and ocean acidification using the novel Li/Mg-SST and δ^{11}B-pH proxies in the Caribbean coral *Siderastrea siderea*, Doctoral thesis, University of Southampton, 2017.

Fowell, S. E., Sandford, K., Stewart, J. A., Castillo, K. D., Ries, J. B., and Foster, G. L.: Intrareef variations in Li/Mg and Sr/Ca sea surface temperature proxies in the Caribbean reef-building coral *Siderastrea siderea*, Paleoceanography, 31, 1315–1329, https://doi.org/10.1002/2016PA002968, 2016.

Fritz, H. M., Blount, C. D., Albusaidi, F. B., and Al Harthy, A. H. M.: Cyclone Gonu storm surge in Oman, Estuar. Coast. Shelf S., 86, 102–106, https://doi.org/10.1007/978-90-481-3109-9_30, 2010.

Garbe-Schönberg, D. and Müller, S.: Nano-particulate pressed powder tablets for LA-ICP-MS, J. Anal. Atom. Spectrom., 29, 990–1000, https://doi.org/10.1039/C4JA00007B, 2014.

Garcia, H. E., Weathers, K. W., Paver, C. R., Smolyar, I., Boyer, T. P., Locarnini, R. A., Zweng, M. M., Mishonov, A. V., Baranova, O. K., Seidov, D., and Reagan, J. R.: World Ocean Atlas 2018. Vol. 4: Dissolved Inorganic Nutrients (phosphate, nitrate and nitrate + nitrite, silicate), A. Mishonov Technical Editor, NOAA Atlas NESDIS 84, 35 pp., 2019.

Glynn, P.: Coral growth in upwelling and nonupwelling areas off the Pacific coast of Panama, J. Mar. Res., 35, 567–585, 1977.

Glynn, P. W.: Monsoonal upwelling and episodic *Acanthaster* predation as probable controls of coral reef distribution and community structure in Oman, Indian Ocean, Atoll Research Bulletin, 379, 1–66, https://doi.org/10.5479/si.00775630.379.1, 1993.

Grigg, W. G.: Coral reef development at high latitudes in Hawaii, Proceedings of the Fourth International Coral Reef Symposium, 18–22th May 1981, Manila, 1, 688–693, 1981.

Guan, Y., Hohn, S., Wild, C., and Merico, A.: Vulnerability of global coral reef habitat suitability to ocean warming, acidification and eutrophication, Glob. Change Biol., 26, 5646–5660, https://doi.org/10.1111/gcb.15293, 2020.

Hall, E. R., Muller, E. M., Goulet, T., Bellworthy, J., Ritchie, K. B., and Fine, M.: Eutrophication may compromise the resilience of the Red Sea coral Stylophora pistillata to global change, Mar. Pollut. Bull., 131, 701–711, https://doi.org/10.1016/j.marpolbul.2018.04.067, 2018.

Hallock, P.: The role of nutrient availability in bioerosion: Consequences to carbonate buildups, Palaeogeogr. Palaeocl., 63, 275–291, https://doi.org/10.1016/0031-0182(88)90100-9, 1988.

Hastenrath, S. and Greischar, L.: The monsoonal current regimes of the tropical Indian Ocean: Observed surface fields and their geostrophic and wind-driven components, J. Geophys. Res., 96, 12619–12633, https://doi.org/10.1029/91JC00997, 1991.

Hathorne, E. C., Felis, T., Suzuki, A., Kawahata, H., and Cabioch, G.: Lithium in the aragonite skeleton of massive *Porites* corals: A new tool to reconstruct tropical sea surface temperatures, Paleoceanography, 28, 143–152, https://doi.org/10.1029/2012PA002311, 2013.

Helmle, K. P., Kohler, K. E., and Dodge, R. E.: The coral X-radiograph densitometry system: CoralXDS, Nova Southeastern University, Fort-Lauderdale-Davie, 2002.

Helmle, K. P., Dodge, R. E., Swart, P. K., Gledhill, D. K., and Eakin, C. M.: Growth rates of Florida corals from 1937 to 1996 and their response to climate change, Nat. Commun., 2, 215–216, https://doi.org/10.1038/ncomms1222, 2011.

Highsmith, R. C.: Coral growth rate and environmental control of density banding, J. Exp. Mar. Biol. Ecol. 37, 105–125, https://doi.org/10.1016/0022-0981(79)90089-3, 1979.

Howells, E. J., Abrego, D., Vaughan, G. O., and Burt, J. A.: Coral spawning in the Gulf of Oman and relationship to latitudinal variation in spawning season in the northwest Indian Ocean, Sci. Rep., 4, 1–6, https://doi.org/10.1038/srep07484, 2014.

Hughes, T. P., Barnes, M. L., Bellwood, D. R., Cinner, J. E., Cumming, G. S., Jackson, J. B. C., Kleypas, J., van de Leemput, I. A., Lough, J. M., Morrison, T. H., Palumbi, S. R., van Nes, E. H., and Scheffer, M.: Coral reefs in the Anthropocene, Nature, 546, 82–90, https://doi.org/10.1038/nature22901, 2017.

Inoue, M., Suzuki, A., Nohara, M., Hibino, K., and Kawahata, H.: Empirical assessment of coral Sr/Ca and Mg/Ca ratios as climate proxies using colonies grown at different temperatures, Geophys. Res. Lett., 34, 1–4, https://doi.org/10.1029/2007GL029628, 2007.

Jiang, Q., Cao, Z., Wang, D., Li, Y., Wu, Z., and Ni, J.: Coral Ba/Ca and Mn/Ca ratios as proxies of precipitation and terrestrial input at the eastern offshore area of Hainan Island, J. Ocean U. China, 16, 1072–1080, https://doi.org/10.1007/s11802-017-3265-0, 2017.

Jochum K. P., Willbold M., Raczek I., Stoll B., and Herwig K.: Chemical characterisation of the USGS reference glasses GSA-1G, GSC-1G, GSD-1G, GSE-1G, BCR-2G, BHVO- 2G and BIR-1G using EPMA, ID-TIMS, ID-ICP-MS and LA- ICP-MS, Geostand. Geoanal. Res., 29, 285–302, https://doi.org/10.1111/j.1751-908X.2005.tb00901.x, 2005.

Jochum, K. P., Stoll, B., Herwig, K., and Willbold, M.: Validation of LA-ICP-MS trace element analysis of geological glasses using a new solid-state 193 nm Nd : YAG laser and matrix-matched calibration, J. Anal. Atom. Spectrom., 22, 112–121, https://doi.org/10.1039/b609547j, 2007.

Jochum K. P., Weis U., Stoll B., Kuzmin D., Yang Q., Raczek I., Jacob D. E., Stracke A., Birbaum K., Frick D. A., Guenther D., and Enzweiler J.: Determination of reference values for NIST SRM 610–617 glasses following ISO guidelines, Geostand. Geoanal. Res., 35, 397–429, https://doi.org/10.1111/j.1751-908X.2011.00120.x, 2011.

JPL MUR MEaSUREs Project: GHRSST Level 4 MUR Global Foundation Sea Surface Temperature Analysis, Ver. 4.1. PO.DAAC [data set], CA, USA, https://doi.org/10.5067/GHGMR-4FJ04, 2015.

Klein, R. and Loya, Y.: Skeletal growth and density pattern of two *Porites* corals from the Gulf of Eilat, Red Sea, Mar. Ecol. Prog. Ser., 77, 253–259, https://doi.org/10.3354/meps077253, 1991.

Kleypas, J. A., McManus, J. W., and Meñez, L. A. B.: Environmental limits to coral reef development: Where do we draw the line?, Am. Zool., 39, 146–159, https://doi.org/10.1093/icb/39.1.146, 1999.

Knutson, D. W., Buddemeier, R. W., and Smith, S. V.: Coral chronometers: Seasonal growth bands in reef corals, Science, 177, 270–272, https://doi.org/10.1126/science.177.4045.270, 1972.

Koop, K., Booth, D., Broadbents, A., Brodie, J., Bucher, D., Capone, D., Coll, J., Dennison, W., Erdmann, M., Harrison, P., Hoegh-Guldberg, O., Hutchings, P., Jones, G. B., Larkum, A. W. D., O'Neil, J., Steven, A., Tentori, E., Ward, S., Williamson, J., and Yellowless, D.: ENCORE: The effect of nutrient enrichment on coral reefs. Synthesis of results and conclusions, Mar. Pollut. Bull., 42, 91–120, https://doi.org/10.1016/S0025-326X(00)00181-8, 2001.

Lapointe, B. E. and Clark, M. W.: Nutrient inputs from the watershed and coastal eutrophication in the Florida Keys, Estuaries, 15, 465–476, https://doi.org/10.2307/1352391, 1992.

Lea, D. W., Shen, G. T., and Boyle, E. A.: Coralline barium records temporal variability in equatorial Pacific upwelling, Nature, 340, 373–376, https://doi.org/10.1038/340373a0, 1989.

Lee, C. M., Jones, B. H. Brink, K. H., and Fischer, A. S.: The upper-ocean response to monsoonal forcing in the Arabian Sea: seasonal and spatial variability, Deep-Sea Res. Pt. II, 47, 1177–1226, https://doi.org/10.1016/S0967-0645(99)00141-1, 2000.

Locarnini, R. A., Mishonov, A. V., Baranova, O. K., Boyer, T. P., Zweng, M. M., Garcia, H. E., Reagan, J. R., Seidov, D., Weathers, K., Paver, C. R., and Smolyar, I.: World Ocean Atlas 2018, Volume 1: Temperature, A. Mishonov Technical Ed., NOAA Atlas NESDIS 81, 52 pp., 2018.

Logan, A. and Tomascik, T.: Extension growth rates in two coral species from high-latitude reefs of Bermuda, Coral Reefs, 10, 155–160, 1991.

Lough, J. M. and Barnes, D. J.: Environmental controls on growth of the massive coral *Porites*, J. Exp. Mar. Biol. Ecol., 245, 225–243, https://doi.org/10.1016/s0022-0981(99)00168-9, 2000.

Lough, J. M., Cantin, N. E., Benthuysen, J. A., and Cooper, T. F.: Environmental drivers of growth in massive *Porites* corals over 16 degrees of latitude along Australia's northwest shelf, Limnol. Oceanogr., 61, 684–700, https://doi.org/10.1002/lno.10244, 2016.

Manzello, D. P., Enochs, I. C., Bruckner, A., Renaud, P. G., Kolodziej, G., Budd, D. A., Carlton, R., and Glynn, P. W.: Galápagos coral reef persistence after ENSO warming across an acidification gradient, Geophys. Res. Lett., 41, 9001–9008, https://doi.org/10.1002/2014GL062501, 2014.

Manzello, D. P., Enochs, I. C., Kolodziej, G., and Carlton, R.: Recent decade of growth and calcification of *Orbicellla faveolata* in the Florida Keys: an inshore-offshore comparison, Mar. Ecol. Prog. Ser., 521, 81–89, https://doi.org/10.3354/meps11085, 2015.

McCulloch, M. T., D'Olivo, J. P., Falter, J., Holcomb, M., and Trotter, J. A.: Coral calcification in a changing world and the interactive dynamics of pH and DIC upregulation, Nat. Commun., 8, 1–8, https://doi.org/10.1038/ncomms15686, 2017.

Mertz-Kraus, R., Brachert, T. C., Jochum, K. P., Reuter, M., and Stoll, B.: LA-ICP-MS analyses on coral growth increments reveal heavy winter rain in the Eastern Mediterranean at 9 Ma, Palaeogeogr. Palaeocl., 273, 25–40, https://doi.org/10.1016/j.palaeo.2008.11.015, 2009.

Mischel, S. A., Mertz-Kraus, R., Jochum, K. P., and Scholz, D.: TERMITE: An R script for fast reduction of laser ablation inductively coupled plasma mass spectrometry data and its application to trace element measurements, Rapid Commun. Mass Sp., 31, 1079–1087, https://doi.org/10.1002/rcm.7895, 2017.

Mollica, N. R., Guo, W., Cohen, A. L., Huang, K., Foster, G. L., Donald, H. K., and Solow, A. R.: Ocean acidification affects coral growth by reducing skeletal density, P. Natl. Acad. Sci. USA, 115, 1754–1759, https://doi.org/10.1073/pnas.1712806115, 2018.

Montaggioni, L. F., Le Cornec, F., Corrège, T., and Cabioch, G.: Coral barium/calcium record of mid-Holocene upwelling activity in New Caledonia, South-West Pacific, Palaeogeogr. Palaeocl., 237, 436–455, https://doi.org/10.1016/j.palaeo.2005.12.018, 2006.

Montagna, P., McCulloch, M., Douville, E., López Correa, M., Trotter, J., Rodolfo-Metalpa, R., Dissard, D., Ferrier-Pagès, C., Frank, N., Freiwald, A., Godstein, S., Mazzoli, C., Reynaud, S., Rüggeberg, A., Russo, S., and Taviani, M.: Li/Mg systematics in scleractinian corals: Calibration of the thermometer, Geochim. Cosmochim. Ac., 132, 288–310, https://doi.org/10.1016/j.gca.2014.02.005, 2014.

Muscatine, L. and Porter, J. W.: Reef Corals: Mutualistic Symbioses Adapted to Nutrient-Poor Environments, Bioscience, 27, 454–460, https://doi.org/10.2307/1297526, 1977.

Muscatine, L., McCloskey, L. R., and Marian, R. E.: Estimating the daily contribution of carbon from zooxanthellae to coral animal respiration, Limnol. Oceanogr., 26, 601–611, https://doi.org/10.4319/lo.1981.26.4.0601, 1981.

NCEI (National Centers for Environmental Information): World Ocean Atlas 2018 (WOA18), NCEI [data set], https://www.nodc.noaa.gov/OC5/woa18/woa18data.html, last access: 26 July 2022.

Okai, T., Suzuki, A., Kawahata, H., Terashima, S., and Imai, N.: Preparation of a new Geological Survey of Japan geochemical reference material: Coral JCp-1, Geostandard. Newslett., 26, 95–99, https://doi.org/10.1111/j.1751-908X.2002.tb00627.x, 2002.

Omer, W. M. M.: Ocean acidification in the Arabian Sea and the Red Sea – factors controlling pH, Unpublished master's thesis, Universitas Bergensis, 2010.

Paillard, D., Labeyrie, L., and Yiou, P.: Macintosh program performs time-series analysis, EOS T. Am. Geophys. Un., 77, 379, https://doi.org/10.1029/96EO00259, 1996.

Perry, C. T., Edinger, E. N., Kench, P. S., Murphy, G. N., Smithers, S. G., Steneck, R. S., and Mumby, P. J.: Estimating rates of biologically driven coral reef framework production and erosion: A new census-based carbonate budget methodology and applications to the reefs of Bonaire, Coral Reefs, 31, 853–868, https://doi.org/10.1007/s00338-012-0901-4, 2012.

Quinn, N. J. and Johnson, D. W.: Cold water upwellings cover Gulf of Oman coral reefs, Coral Reefs, 15, 214, 1996.

Ross, C. L., DeCarlo, T. M., and McCulloch, M. T.: Environmental and physiological controls on coral calcification along a latitudinal temperature gradient in Western Australia, Glob. Change Biol., 25, 431–447, https://doi.org/10.1111/gcb.14488, 2019a.

Ross, C. L., DeCarlo, T. M., and McCulloch, M. T.: Calibration of Sr/Ca, Li/Mg and Sr-U paleothermometry in branching and foliose corals, Paleoceanogr. Paleoclimatol., 34, 1271–1291, https://doi.org/10.1029/2018PA003426, 2019b.

Salm, R. V.: Coral reefs of the Sultanate of Oman, Atoll Research Bulletin., 380, 1–85, https://doi.org/10.5479/si.00775630.380.1, 1993.

Scoffin, T. P., Tudhope, A. W., Brown, B. E., Chensang, H., and Cheeney, R. F.: Patterns and possible environmental controls of skeletogenesis of *Porites lutea*, South Thailand, Coral Reefs, 11, 1–11, https://doi.org/10.1007/BF00291929, 1992.

Smith, R. L. and Bottero, J. S.: On upwelling in the Arabian Sea, in: A Voyage of Discovery, edited by: Angel, M., 70th Anniversary Volume, Pergamon, Tarrytown, N. Y., 291–304, 1977.

Smith, S. L.: Understanding the Arabian Sea: Reflections on the 1994-1996 Arabian Sea expedition, Deep-Sea Res. Pt. II, 48, 1385–1402, https://doi.org/10.1016/S0967-0645(00)00144-2, 2001.

Sun, D., Su, R., McConnaughey, T. A., and Bloemendal, J.: Variability of skeletal growth and δ^{13}C in massive corals from the South China Sea: Effects of photosynthesis, respiration and human activities, Chem. Geol., 255, 414–425, https://doi.org/10.1016/j.chemgeo.2008.07.012, 2008.

Swallow, J. C. and Bruce, J. G.: Current measurements off the Somali coast during the southwest monsoon of 1964, Deep-Sea Res., 13, 861–888, https://doi.org/10.1016/0011-7471(76)90908-6, 1966.

Takahashi, T., Sutherland, S. C., Chipman, D. W., Goddard, J. G., and Ho, C.: Climatological distributions of pH, pCO_2, total CO_2, alkalinity, and $CaCO_3$ saturation in the global surface ocean, and temporal changes at selected locations, Mar. Chem., 164, 95–125, https://doi.org/10.1016/j.marchem.2014.06.004, 2014.

Tanaka, K., Holcomb, M., Takahashi, A., Kurihara, H., Asami, R., Shinjo, R., Sowa, K., Rankenburg, K., Watanabe, T., and McCulloch, M.: Response of *Acropora digitifera* to ocean acidification: constrains from δ^{11}B, Sr, Mg, and Ba composition of aragonitic skeletons cultured under variable seawater pH, Coral Reefs, 34, 1139–1149, https://doi.org/10.1007/s00338-015-1319-6, 2015.

Tomascik, T.: Growth rates of two morphotypes of *Montastrea annularis* along a eutrophication gradient, Barbados, W. I., Mar. Pollut. Bull., 21, 376–381, https://doi.org/10.1016/0025-326X(90)90645-O, 1990.

Tomascik, T. and Sander, F.: Effects of eutrophication on reef-building corals, Mar. Biol., 87, 143–155, https://doi.org/10.1016/0198-0254(87)90298-6, 1985.

Tudhope, A. W., Lea, D. W., Shimmield, G. B., Chilcott, C. P., and Head, S.: Monsoon climate and Arabian Sea coastal upwelling recorded in massive corals from southern Oman, Palaios, 11, 347–361, https://doi.org/10.2307/3515245, 1996.

Vermeij, M. J. A., van Moorselaar, I., Engelhard, S., Hörnlein, C., Vonk, S. M., and Visser, P. M.: The effect of nutrient enrichment and herbivore abundance on the ability of turf algae to overgrow coral in the Caribbean, PLoS One, 5, 1–8, https://doi.org/10.1371/journal.pone.0014312, 2010.

Wellington, G. M. and Glynn, P. W.: Environmental influences on skeletal banding in Eastern Pacific (Panama) corals, Coral Reefs, 1, 215–222, https://doi.org/10.1007/BF00304418, 1983.

Wilson, S.: Ecology of coral communities in a marginal environment: Southern Arabia, Unpublished doctoral thesis, University of Warwick, https://doi.org/10.13140/RG.2.2.26085.40164, 2007.

Wizemann, A., Nandini, S. D., Stuhldreier, I., Sánchez-Noguera, C., Wisshak, M., Westphal, H., Rixen, T., Wild, C., and Reymond, C. E.: Rapid bioerosion in a tropical upwelling coral reef, PLoS One, 13, 1–22, https://doi.org/10.1371/journal.pone.0202887, 2018.

Zinke, J., D'Olivo, J. P., Gey, C. J., McCulloch, M. T., Bruggemann, J. H., Lough, J. M., and Guillaume, M. M. M.: Multi-trace-element sea surface temperature coral reconstruction for the southern Mozambique Channel reveals teleconnections with the tropical Atlantic, Biogeosciences, 16, 695–712, https://doi.org/10.5194/bg-16-695-2019, 2019.